Available online at www.sciencedirect.com
SCIENCE DIRECT®
International Journal of Heat and Mass Transfer 49 (2006) 4624–4632
International Journal of HEAT and MASS TRANSFER
www.elsevier.com/locate/ijhmt

An inverse heat transfer method to provide near-isothermal surface for disc heaters used in microlithography

Arunn Narasimhan *, Satish Karra

Heat Transfer and Thermal Power Laboratory, Department of Mechanical Engineering, Indian Institute of Technology Madras, Chennai 600 036, India

Received 2 September 2005; received in revised form 6 April 2006
Available online 27 June 2006

Abstract

In microlithography, the fabrication method for semiconductors and MEMS devices, the post-exposure baking process involves the baking (heating) of a 300 mm diameter, ~1 mm thick silicon wafer substrate with a disc heater to a set point temperature (T_{SET}) triggering the photo-chemical reaction undergone by the photo-resist applied on the wafer. For a known loss occurring due to the convection boundary conditions at the top and side of the disc heater surface, providing a steady state heat power (Q_T, W) as a constant heat flux (q'', W/m^2) over the heater bottom surface (A, m^2) would result in a fixed temperature difference ΔT (=$T_{MAX} - T_{MIN}$) on the heater top surface. Minimizing this heater surface ΔT – an imprint of which is transferred to the heated wafer – is crucial for determining the accuracy of the semiconductor circuit pattern etched on the silicon wafer. To reduce this ΔT further ($\Delta T \rightarrow \Delta T_{MIN}$) for identical steady state heat power Q_T, a cost-effective method of two-zone redistribution of the heater bottom surface heat fluxes (two heat fluxes q_1'' and q_2'' given, respectively, to the inner and the outer-zones) is proposed. This inverse heat transfer problem in steady state is verified using numerical methods and scaling analysis from first principles. For given convection heat losses and T_{SET}, the achievable heater surface ΔT_{MIN} decreases as the split radius increases. Also, there exists a critical split radius (r_c) below which no energy need be given to the inner-zone to achieve ΔT_{MIN} (i.e., $q_1'' = 0$). This r_c value is predicted using the theoretical scaling analysis and was found to match excellently with the value obtained from numerical methods. The variations of heater surface ΔT, q_1''/q_2'', and r_c were found to be independent of the T_{SET} and dependent only on the heat losses. Limiting values of achievable heater surface ΔT_{MIN} for various split locations dividing the two-zones of heat flux are also presented.

Keywords: Microlithography; Silicon wafer; Post-exposure bake; Inverse heat transfer; Temperature uniformity; Scale analysis

1. Introduction

Microlithography, a semiconductor manufacturing process, has been used extensively for printing circuit patterns on silicon wafers, semiconductor devices like diodes, transistors, integrated circuits and in the fabrication of MEMS devices used in sensors, actuators and biomedical devices [1–3]. Microlithography involves the deposition, baking and exposure of a photo-resist for building a pattern, and a developing process for washing away the unexposed photo-resist (for positive-imaging resists). A flowchart of the sequential photo-lithography process steps followed almost unaltered in the microlithography industry for the past two decades [1,2] is given in Table 1.

In the present-day industry-standard DUV irradiated, photo-resist lithography process, [4,5], as described in the initial processes of Table 1, the film of polymeric resist is exposed to patterned UV radiation, creating an image of the acid pattern (integrated circuitry) in the film. A subsequent heating step denoted in step 8 of Table 1 as post-exposure bake (PEB) process, alters the solubility of the acidic pattern in the irradiated portions of the film [6]. This allows the desired single layer three-dimensional relief pattern to be retained on the photo-resist film, after subjecting to the develop process in Table 1. The accuracy of circuit patterns generated by the photo-lithography process is assessed using a representative 'critical dimension' (CD)

* Corresponding author. Tel.: +91 44 225 74696; fax: +91 44 225 78501.
E-mail address: arunn@iitm.ac.in (A. Narasimhan).

0017-9310/$ - see front matter © 2006 Elsevier Ltd. All rights reserved.
doi:10.1016/j.ijheatmasstransfer.2006.04.019

Nomenclature

A	surface area (m^2)
CD	critical dimension
DUV	deep ultra-violet
h	heat transfer coefficient (W/m^2 K)
k	thermal conductivity (W/m K)
MEMS	microelectro-mechanical systems
PEB	post-exposure bake
q''	heat flux (W/m^2)
Q	energy (W)
r	radial co-ordinate, radius (mm)
R	radius of the heater (mm) (=150 mm), Fig. 1
t	thickness of the heater (mm) (=30 mm), Fig. 1
T	temperature (°C)
ΔT	dimensional temperature difference, Eq. (1) (°C)
z	axial co-ordinate (mm)

Greek symbols

θ	non-dimensional temperature, Eq. (8)
$\Delta\theta$	non-dimensional temperature difference

Subscripts

amb, ∞	ambient
c	critical
e	average of the heater side
MIN	minimum
MAX	maximum
r	quantity pertaining to radial direction
SET	set point
T	total
z	quantity pertaining to axial direction
1	quantity pertaining to inner-zone, Fig. 1(b)
2	quantity pertaining to outer-zone, Fig. 1(b)

Table 1
Sequence of microlithography manufacturing process steps

Step	Operation	Manufacturing processes
1	Substrate preparation	Oxidation, chemical vapor deposition, etc.
2	Surface preparation	Clean, dehydrate, prime, etc.
3	Application of resist	Spin coating, spraying, rolling, dipping, etc.
4	Soft bake	Low temperature cure to dry resist
5	Expose	Align and expose to selectively polymerize the resist
6	Development	Dissolve the un-polymerized resist
7	Visual inspection	Verify accurate image transfer to photo-resist
8	Post-exposure bake	Higher temperature cure to completely dry and polymerize the resist
9	Etch	Surface, oxide, metal, etc.
10	Strip resist	Organic, acid, or plasma ash removal of resist
11	Visual inspection	Verify accurate image transfer to the layer

measured or estimated in terms of the smallest line-width of the patterned feature on the photo-resist [1,2]. The temperature uniformity of the photo-resist and hence the bake-heater surface itself, during the above mentioned PEB plays a key role in determining the uniformity of photo-resist thickness or CD [3,5–7] for subsequent unit processes such as etching, ion-implantation or deposition, leading to a successful (accurate) manufacture of the semiconductor.

Using numerical methods and theoretical scale analysis from first principles, this paper presents a parametric study of an inverse heat conduction problem (IHCP, [8]) on the axi-symmetric model of a disc heater that maintains a given temperature on its top surface (on which the wafer is heated) for a given length of time. A cost-effective two-zone circumferential redistribution of the heat flux at the bottom surface of the heater is studied in detail to counter the two opposing constraints of the problem: the requirement of a minimum possible heater surface ΔT and the fixed heat losses to the surrounding, which is the cause for the ΔT on the heater surface.

2. Temperature uniformity requirement

The baking (heating) process, performed on several occasions (step 4, 8 and after 9 in Table 1) in the microlithography manufacturing of semiconductors, is done by placing the silicon wafer on a heater, usually made of aluminum [9]. Fig. 1(a) shows the axi-symmetric schematic of a 300 mm diameter wafer placed on a disc heater. The photo-chemistry of the chemical bond, hardening or softening of the photo-resist applied on the wafer, is highly sensitive to a set point temperature (T_{SET}) to be reached by PEB, upon which the chemical reaction is triggered (chemical amplification, [4]). The accuracy of the feature dimensions of the semiconductor circuit pattern to be etched on the wafer depends sensitively on the uniformity of these

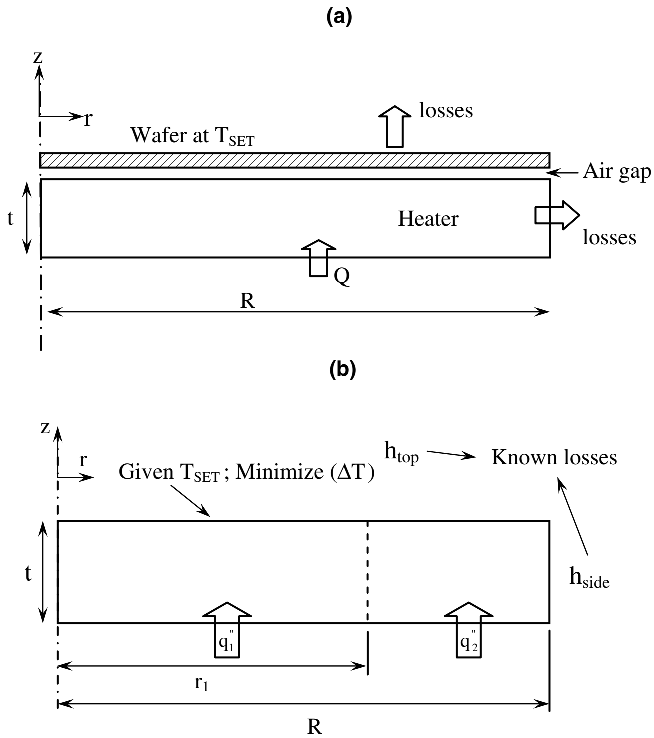

Fig. 1. (a) Axi-symmetric schematic of a semiconductor wafer and heater disc; (b) Schematic showing the method of heat flux re-distribution by splitting the heater disc into two-zones.

photo-chemical reactions on the photo-resist coated on the wafer [5,7]. This in turn depends on the spatial temperature uniformity on the thin (~1 mm) wafer surface, which is a direct imprint of the temperature uniformity of the top surface of the baking heater (Fig. 1(a)) of larger thermal mass [10,6]. This is true only when the natural convection effect from the top and side of the wafer substrate considered in [11–13] are eliminated. This can be done by providing a sealed container with proper size within which the baking is carried out. As shown in [9,14,15], the top and side lid of such a container are to be designed such that the air gap between them and the wafer top surface is small enough to prevent natural convection.

Hence, the requirement of a cost-effective method from the semiconductor industry, to minimize the heater surface ΔT, while baking the wafer at a T_{SET} led to a lot of research in this field in the past few years. For instance, Ho et al. [12,16] proposed an optimal control scheme to maintain the steady state wafer surface temperature at the set-point temperature. Tan and Li [17] described a method for in situ estimation of the temperature sensor parameters, and proposed an algorithm for post-processing the sensor output to improve temperature measurement accuracy, to maintain stringent temperature conditions. Tay et al. [13,18] developed an integrated bake/chill module with in situ temperature measurement capability for the baking of 300 mm silicon wafers, which gives better control over the substrate temperature. Three dimensional numerical simulation studies and experimental verification on a combination bake-chill station were done by Narasimhan et al. [19] and Narasimhan and Ramanan [9], addressing the thermal agility capability of disc heaters to reach and maintain the wafer at different T_{SET} values (for triggering various combinations of photo-resists on the wafer surface) and bring the temperature back to clean room temperature (by chilling/cooling process) within the prescribed bake-chill cycle time of 150 s. Temperature uniformity of the heater surface was addressed only marginally.

3. Inverse heat conduction method

With reference to Fig. 1 it is clear that the temperature of the heater top surface (in principle the entire heater block) will be spatially uniform only if the top and side heat losses to the surrounding are suitably 'compensated' by the energy crossing as heat at the bottom surface of the heater. A method of solution is to 'profile' the heat flux spatially and/or temporally to achieve a particular temperature boundary condition (T_{SET}), in other words, one needs to solve an inverse heat transfer problem [8]. For instance, Huang et al. [20] applied two-dimensional inverse analysis utilizing the conjugate gradient method of minimization to estimate the surface thermal behavior (i.e. heat flux and temperature) of a steel mill roll and Park and Jung [21] used Karhunen–Loève Galerkin procedure for an efficient recursive method to solve the IHCP of estimating the wall heat flux on the wafer from the measurements of wafer temperature in rapid thermal processing, another method used to manufacture semiconductors, where precise control of wafer temperature by adjusting wall heat flux is required.

The above two examples are inherently unsteady, while Cole and Yen [22] solved the IHCP for a rectangle under steady state condition using Green's function. The present problem can also be solved in a steady state domain for the following reasons. Although transient effects could affect the CD uniformity to an extent [11,12], the photo-chemistry and hence the CD accuracy is more sensitive only after the wafer reaches the amplification threshold of T_{SET} [10]. Hence the 120 s baking process is done in two phases. In order to reach the T_{SET} in such short time, a large heat load (of the order of 50 000 W/m^2) is given in the first 30 s of the baking process. This step is followed by a steady state heat 'compensation', using feedback control of the heat input to the heater as done in [9,14,15], to maintain the T_{SET} for the remaining of the 90 s. Minimum temperature non-uniformity is required only in these 90 s because of the temperature sensitivity of the triggered photo-chemistry. Hence, in this second baking phase, for the heater (and the wafer on top of it) to remain at a particular T_{SET}, the 'heat input compensation' should be achieved by spatially redistributing the fixed quantity of energy crossing into the heater from the bottom, for analyzing which, a steady state formulation is sufficient. Although the simulations in this paper were to be performed in the direct approach (i.e., provide heat flux that results in a temperature distribution), the objective of the problem here is to find a steady state heat flux distribution that could result in a known, near iso-thermal top surface in a disc. In this sense, it is reasonable to classify this problem as an inverse heat transfer problem.

4. Method of heat flux re-distribution

Because of the negligible wafer thickness (∼1 mm) when compared to the heater thickness (30 mm, for 'thin' bake plates [10], which is used in this study), simulation studies [23] have shown that the thermal resistance of the air in the proximity gap (see Fig. 1(a)) allows the lateral conduction in the wafer, improving the temperature uniformity of the wafer. Further, it has been shown that for a uniform proximity distance (air gap thickness) with a uniform heat loss, the wafer surface temperature non-uniformity is always less than that of the heater. Hence, with an assumed constant proximity gap distance between the wafer and the heater top surface, it is sufficient to consider minimizing the heater surface temperature non-uniformity. Further, although the heat loss from the heater with and without the wafer on top could be different, it will not affect the results of this paper, as the heat loss can be linearly compensated in the total heat input given to the heater from the bottom, as will be seen in Sections 7 and 8. To maintain the heater top surface at T_{SET}, a steady state energy, Q_T (W), in the form of heat flux, q''_T (W/m^2), is provided over an area, A (m^2) by a thin resistor strip attached to the heater bottom. Radiation heat losses from the heater can be neglected as their relative magnitude with respect to the conduction flux was shown [2] only to be a small fraction. Assuming the heater surface to be flat with negligible bottom surface heat losses, a circumferentially uniform convection heat transfer losses (see Fig. 1(a)) from the heater would then set a temperature difference on the heater surface:

$$\Delta T = T_{MAX} - T_{MIN} \tag{1}$$

where T_{MAX} and T_{MIN} are the maximum and minimum temperatures on the heater surface.

A method to determine $q''(r)$, which minimizes ΔT, is to split the heater disc into two-zones, the inner circular-zone with radius 'r_1' and the outer annular-zone ($r_2 = R - r_1$) as shown in Fig. 1(b). For a chosen T_{SET}, the required steady state heat power Q_T to compensate for the convection losses (applicable in the 90 s second phase of the PEB) is provided by two heat fluxes q''_1 and q''_2 given respectively to the inner and the outer-zones. For a given T_{SET} and particular location of the 'split' determined by r_1, q''_1 and q''_2 given at the bottom surface are varied such that the energy given Q_T remains constant, seeking a minimum value for the prevailing ΔT on the top surface of the heater. In order to execute and analyze the above objective, the steady state energy equation for the axi-symmetric configuration shown in Fig. 1(b) can be written as:

$$\frac{1}{r}\frac{\partial}{\partial r}\left(r\frac{\partial T}{\partial r}\right) + \frac{\partial^2 T}{\partial z^2} = 0 \tag{2}$$

with the boundary conditions

$$\frac{\partial T}{\partial r} = 0 \text{ at } r = 0; \quad -k\frac{\partial T}{\partial r} = h_{side}(T - T_{amb}) \text{ at } r = R;$$
$$-k\frac{\partial T}{\partial z} = q''_T \text{ at } z = 0 \quad \text{and} \quad -k\frac{\partial T}{\partial z} = h_{top}(T - T_{amb}) \text{ at } z = t. \tag{3}$$

From the proposed method of heat flux re-distribution, the heat flux boundary condition at the bottom of the heater satisfies the following equation:

$$Q_T = q''_T A_T = Q_1 + Q_2 = q''_1 A_1 + q''_2 A_2 \tag{4}$$

which could be re-written as:

$$q''_T = q''_1 (r_1/R)^2 + q''_2\left[1 - (r_1/R)^2\right] \tag{5}$$

where the terms are explained in the nomenclature.

5. Grid independence and numerical methods validation

For a T_{SET} and known uniform convective boundary losses (h_{top}, h_{side}), the steady state energy Q_T (q''_T applied over A_T) required to maintain the average temperature on the heater top surface at T_{SET}, without splitting the disc is found by solving using numerical methods, the finite volume formulation of Eq. (2) subjected to the respective formulation of the boundary conditions in Eqs. (3)–(5). Grid independence study using uniform rectangular grids on the axi-symmetric domain shown in Fig. 1(b) has been performed for $T_{SET} = 90$ °C and the results of minimum temperature for the whole heater is presented in Table 2. Based on these results, a uniform rectangular grid of 150×30 is used for subsequent numerical simulations. Further, the problem of heat transfer inside a circumferential fin (see Fig. 2(a)) is chosen for the validation of the numerical scheme. The analytical solution of the temperature distribution for this configuration is given by [22]:

$$\frac{T(r) - T_{amb}}{T_b - T_{amb}} = \frac{I_0(mr)K_1(mr_2) + K_0(mr)I_1(mr_2)}{I_0(mr_1)K_1(mr_2) + K_0(mr_1)I_1(mr_2)} \tag{6}$$

where

$$m^2 = 2h/kt \tag{7}$$

and I and K are the modified Bessel functions of first and second kind respectively. The radial temperature profile of the disc heater central section ($z = 15$ mm) using the numerical scheme is compared with that obtained using Eq. (6) in Fig. 2(b). The average error is found to be 0.105% thus validating the numerical scheme for sufficient accuracy.

Table 2
Results of grid independence study

Grid	Overall T_{MIN} (°C)	Temp. change in %
60×15	89.54617	
150×30	89.54367	0.0028
300×60	89.54248	0.00138

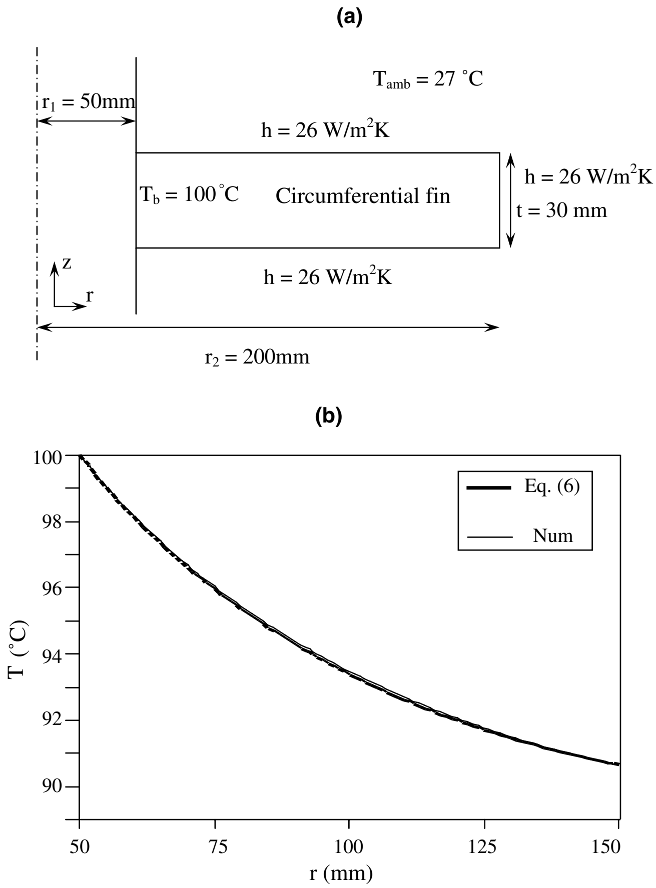

Fig. 2. (a) Axi-symmetric schematic of the circumferential fin problem for the validation of the numerical code; (b) Comparison of the numerical simulation with the mathematical solution.

6. Influence of split location

Considering a average heater top surface $T_{SET} = 90$ °C, and using (from [14]) $h_{top} = 7.5$ W/m^2 K and $h_{side} = 26$ W/m^2 K in Fig. 1(b) as the heat transfer coefficients based on the standard microlithography industry clean room air temperature, the required average heat flux at the bottom of the heater, without splitting it into two-zones (i.e., $q''_T = q''_1$), is found to be 1125 W/m^2. The resulting radial temperature distribution at the top surface is shown in Fig. 3 as the top curve marked as $q''_1 = 1125$ W/m^2, using suitable non-dimensional variables for radial position (r_1/R) and temperature given by:

$$\theta = [T - T_\infty]/[T_{SET} - T_\infty]. \tag{8}$$

From Fig. 3, it can be seen that the $\Delta\theta \sim 0.9$ for the case of the 'one-zone' heater. To reduce further this value of $\Delta\theta$, consider a 'two-zone' heater bottom surface, with the split located at an inner-zone radius, say, $r_1/R = 0.9$. The inner-zone ($0 \leqslant r/R \leqslant 0.9$) heat flux q''_1 is then varied from 0 to q''_T in discrete steps and for each case, the corresponding outer-zone heat flux q''_2 is calculated using Eq. (5). For each given pair of inner and outer-zone heat fluxes (q''_1 and q''_2, satisfying Eq. (5)), given as the boundary conditions for the heater bottom surface, the top surface temperature profile is evaluated using numerical simulations. The rest of the curves in Fig. 3 represent these radial temperature distributions, marked using only q''_1 values. It is clear from these curves that lesser values for $\Delta\theta$ exist at the same energy input Q required to maintain an average T_{SET}, but the energy is made to cross into the heater with a two-zone compensatory heat flux values of q''_1 and q''_2 that satisfies Eq. (5). Fig. 4 depicts graphically the relationship between $\Delta\theta$ and q''_1/q''_T for a given T_{SET} (=90 °C) for the top surface of the heater and split location ($r_1/R = 0.9$) at the bottom surface of the heater. When $q''_1/q''_T = 1$, the $\Delta\theta$ is for the 'one-zone' heater (with $q''_2 = 0$), represented by the right extreme point. Proceeding from *right to left* from this point in Fig. 4, we see that as q''_1/q''_T decreases, $\Delta\theta$ decreases. For the chosen split location ($r_1/R = 0.9$), there exists a unique pair of q''_1 (=301 W/m^2) and q''_2 that satisfies Eq. (5) and

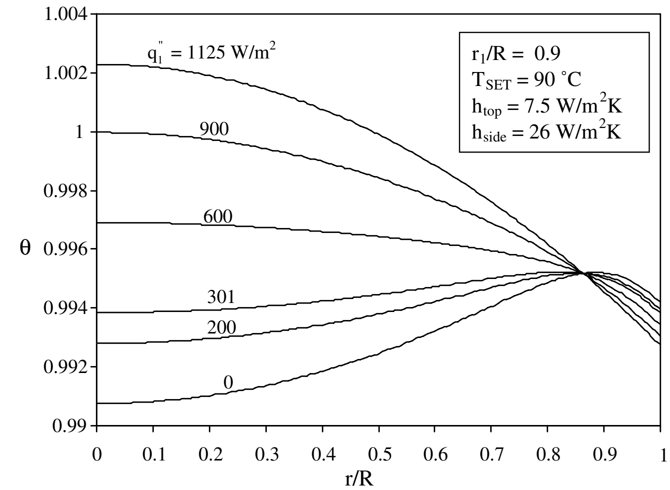

Fig. 3. Temperature profiles on the disc heater surface for various heat flux combinations, for $T_{SET} = 90$ °C, for a split location ($r_1/R = 0.9$).

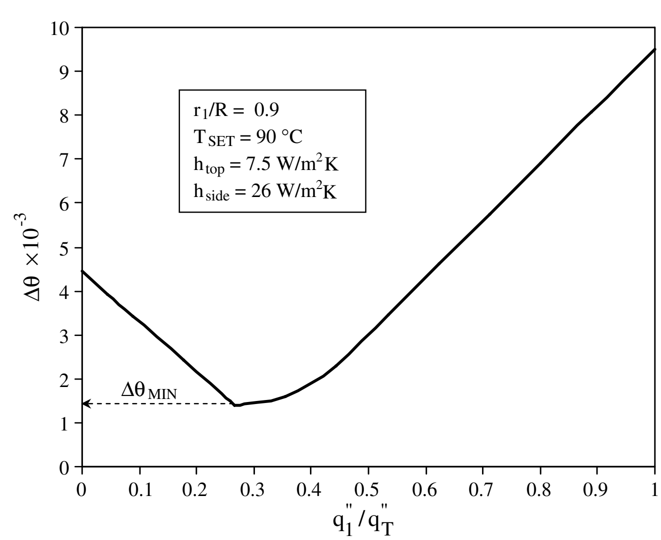

Fig. 4. Variation of heater surface $\Delta\theta$ with q''_1/q''_T for a split location ($r_1/R = 0.9$).

minimizes the surface temperature difference, while maintaining the average heater top surface temperature at the given T_{SET} (=90 °C).

Following the above discussed procedure, from numerical simulation $\Delta\theta$ versus q''_1/q''_T results are plotted for three different split locations in Fig. 5. The first observation from these curves is that irrespective of the split location, when $q''_1/q''_T = 1$ (i.e., when $q''_1 = q''_T$ and $q''_2 = 0$), the $\Delta\theta$ reaches a common maximum value, the same as that for a 'one-zone' heater (see top curve of Fig. 3). It is worth reminding here that the two extreme cases of $r_1/R = 0$ and 1 also mimic a 'one-zone' heater with q''_T provided to the bottom surface and hence would result in a similar common maximum value for $\Delta\theta$ and hence we restrict our analysis to split locations within $0 < r_1/R < 1$. The second and more interesting observation is that as the split location decreases from 0.9 to 0.7, the $\Delta\theta_{MIN}$ increases, while the inner-zone heat flux (q''_1/q''_T) required to achieve this minimum decreases. Extrapolating, we can expect from this observation that when the split location decreases further, there is a critical split location (in this case, $(r_1/R)_c = 0.64$) at and below which, for achieving $\Delta\theta_{MIN}$ no heat flux need be provided to the inner-zone ($q''_1/q''_T = 0$). Hence, in Fig. 5, the curve that connects the $\Delta\theta_{MIN}$ values for each split location becomes a vertical line at the x-axis for $q''_1/q''_T = 0$, with the corresponding increasing $\Delta\theta_{MIN}$ values (y-axis) for each split location $r_1/R \leqslant 0.64$, controlled only by the outer-zone (q''_2) heat flux values.

Further, for a particular value of 'h' and chosen geometry (size) of the heater, the critical split location $(r_1/R)_c$, is found to be independent of the T_{SET}, as shown in Fig. 6, where, in contrast to Fig. 5, the y-axis represents the dimensional temperature difference ΔT. The two curves represent the ΔT_{MIN} for two T_{SET} values, namely, 90 and 120 °C. For both these curves, it can be seen from Fig. 6 that only beyond $r_1/R = 0.64$ a non-zero value for q''_1/q''_T yields lesser ΔT_{MIN} than that of the ΔT_{MIN} value when $q''_1/q''_T = 0$. Fig. 6 portrays this effect using the non-dimensional temperature, θ, Eq. (8), which yields a single curve for the 'h' value used irrespective of the T_{SET} chosen. The reason for the occurrence of the critical split location and its dependence on the various parameters can be explained using a simple but rigorous scale analysis of the problem.

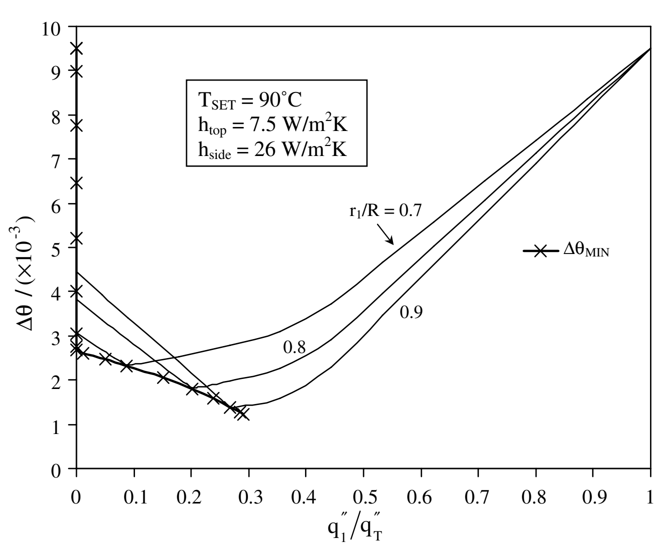

Fig. 5. Variation of heater surface $\Delta\theta$ with q''_1/q''_T for several split locations for $T_{SET} = 90$ °C.

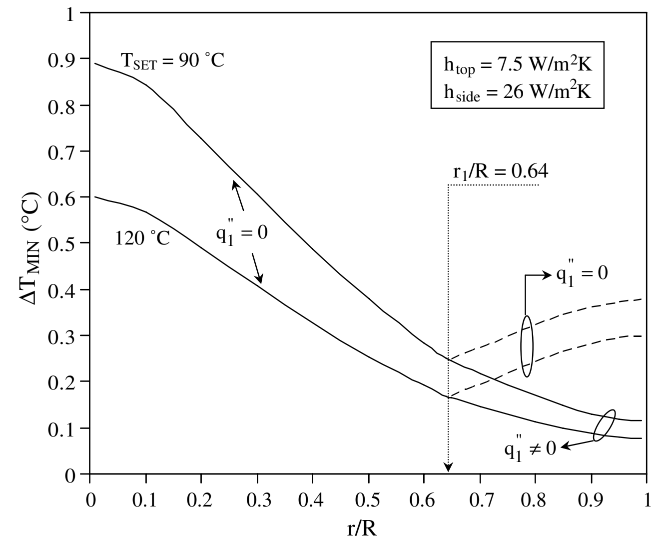

Fig. 6. Heater surface ΔT_{MIN} versus r/R for several split locations for $T_{SET} = 90$ °C and 120 °C.

7. Predicting critical split location using scaling analysis

From the aspect ratio of the problem domain in Fig. 1, it is clear that $\Delta T|_z \ll \Delta T|_r$ as $t \ll R$. Hence, neglecting the heater top surface losses compared to the heater side losses (i.e., setting $h_{top} = 0$), the steady state energy conservation statement with the inner-zone heat flux $q''_1 = 0$ when the heater bottom surface split is located at the critical value $r_c = (r_1/R)_c$, becomes:

$$\begin{aligned} Q_T = q''_T A_T = q''_2 A_2 &= \frac{kA_2}{t}(\Delta T)_z\big|_2 \\ &= 2\pi kt(\Delta T)_r\big|_1 + 2\pi hRt[T_e - T_\infty] \end{aligned} \tag{9}$$

where 'h' is the heat transfer coefficient imposed at the heater edge (=h_{side}) with thickness 't' and T_e is the corresponding edge surface temperature (see Fig. 1(b)). From Eq. (9), the scale for the inner-zone radial temperature difference can be written as:

$$(\Delta T)_r\big|_1 = \frac{Q_T}{2\pi kt} - \frac{hR}{k}[T_e - T_\infty]. \tag{10a}$$

Observe in Eq. (10a), at steady state, Q_T for the problem domain of Fig. 1(b), in general, scales as the sum of the convection losses from the top and side surface of the heater, i.e.,

$$Q_T \sim \left(\pi R^2 h_{top} + 2\pi Rth_{side}\right)[T_e - T_\infty]. \tag{10b}$$

For $q''_1 = 0$ and $q''_2 = q''_T(A_T/A_2)$, the energy balance statement, Eq. (2), can be scaled in the outer-zone as:

$$\frac{(\Delta T)_r|_2}{(R-r)^2} + \frac{(\Delta T)_z|_2}{t^2} = 0 \tag{11}$$

which, upon rearranging yields the scale for the outer-zone radial temperature difference as:

$$(\Delta T)_r|_2 \sim (\Delta T)_z|_2 \left[\frac{R-r}{t}\right]^2. \tag{12}$$

As only the outer-zone is being heated from the bottom until the critical split location $(r_1/R)_c$ (and $q''_1 = 0$), the scale for the axial (z-direction) temperature difference in the outer-zone in Eq. (12) can be found by again invoking the energy balance in Eq. (9), which upon rearranging would result in:

$$\Delta T_z|_2 = \Delta T_r|_1 \left[\frac{2t^2}{R^2 - r^2}\right] + \frac{hR}{k}\left[\frac{2t^2}{R^2 - r^2}\right](T_e - T_\infty) \tag{13}$$

Using Eq. (13) in Eq. (12), results in:

$$\Delta T_r|_2 \sim 2\Delta T_r|_1 \left[\frac{R-r}{R+r}\right] + 2\frac{hR}{k}\left[\frac{R-r}{R+r}\right](T_e - T_\infty). \tag{14}$$

Now we can derive an additional insight that, $\Delta T_r|_2 = \Delta T_r|_1$ at the critical split location $(r_1/R)_c$ as $q''_1 = 0$ and $q''_2 = q''_T(A_T/A_2)$, which would translate (from Eq. (9)) into the diffusion governed inner-zone radial temperature difference being balanced by the diffusion plus convection governed outer-zone temperature difference. Obviously, for a split location $(r_1/R) > (r_1/R)_c$, still setting $q''_1 = 0$ would result in $\Delta T_r|_2 > \Delta T_r|_1$. Hence a non-zero q''_1 'compensates' the inner-zone temperature difference and forces again $\Delta T_r|_2 = \Delta T_r|_1$ to prevail, thus reducing the overall radial temperature difference of the heater top surface as seen from Figs. 6 and 7. Hence to find the critical split location, we set $\Delta T_r|_2 = \Delta T_r|_1$ in Eq. (14), to find:

$$r_c = (r/R)_c = [D-1]/[D+1] \tag{15}$$

where

$$D = 2\left[\frac{Bi}{\Delta T_r|_1}(T_e - T_\infty) + 1\right] \tag{16}$$

with $Bi = hR/k$ can be seen as a characteristic Biot number represented only by the edge heat transfer coefficient (recall we have set $h = h_{side}$), which governs the critical split location. Using a conservative scale for $T_e = (T_{SET} + T_\infty)/2$ along with $h_{top} = 0$ in Eq. (10b) yields Q_T, which can be used in Eq. (10a) to find $\Delta T_r|_1$ the only remaining unknown in Eq. (16).

Taking aluminum as the heater material with $k = 202$ $\mathrm{W m^{-1} K^{-1}}$ and $h_{side} = h = 26\ \mathrm{W m^{-2} K^{-1}}$ (see Fig. 1(b)) along with $R = 150$ mm and $t = 30$ mm for $T_{SET} = 90$ °C and $T_\infty = 30$ °C, using in sequence, Eqs. (10b), (10a), (16) and (15), results in a critical split location $r_c = (r_1/R)_c = 0.635$, which compares excellently with the value of 0.64, obtained through numerical simulations as shown in Fig. 6. The determination of the r_c using Eq. (15), as a function of h_{side} is practically useful for the following reasons. While designing these heaters for using in microlithography manufacturing of microelectronic components, for providing spatially variable heat fluxes, the electric resistance heater-strips of finite thickness are usually laid (wound) as coils with different spatial densities at the bottom surface of the heater. A knowledge of the r_c is always useful to determine the spatial allowances required in the inner and outer-zone electric resistance heater strip densities, for instance, in a two-zone compensatory heater with the split located at a position lesser than the r_c, the entire inner-zone is practically useless for achieving an overall ΔT_{MIN}.

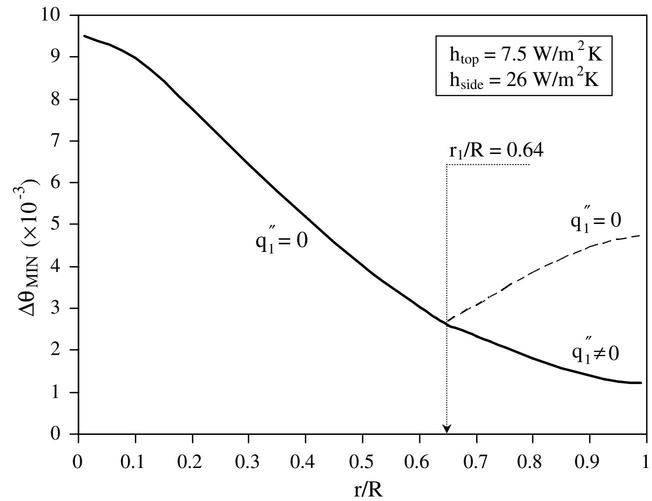

Fig. 7. Heater surface $\Delta\theta_{MIN}$ versus r/R for several split locations for $T_{SET} = 90$ °C and 120 °C.

8. Influence of T_{SET}

Although there is T_e (which is dependent on T_{SET}) in the numerator in Eq. (16), in the denominator there is $\Delta T_r|_1$, which again is dependent on T_e (which is dependent on T_{SET}). Hence the effect of T_{SET} on r_c (predicted from Eq. (15) using Eq. (16)) is null. However, spatial variation in h_{side} could affect the prediction and is not considered in this analysis wherein h_{side} is assumed a constant. This is further validated by the invariant r_c in the numerical simulation results of Figs. 6 and 7, done for two different T_{SET} values, however for identical h_{side} and h_{top} values. The result of an invariant r_c with respect to T_{SET} is again practically useful as this means the same heater can be used for baking the silicon wafer to any T_{SET}, which is governed by the several combinations of the photo-resist and radiation used for imaging the circuit pattern (in general the T_{SET} can vary between 90 and 250 °C, [9,14]). However, the ΔT_{MIN} obtained, as can be seen from Fig. 6, would be different for different T_{SET} values.

Fig. 8 documents graphically, the excellent concurrence of the scale analysis prediction of the critical split location

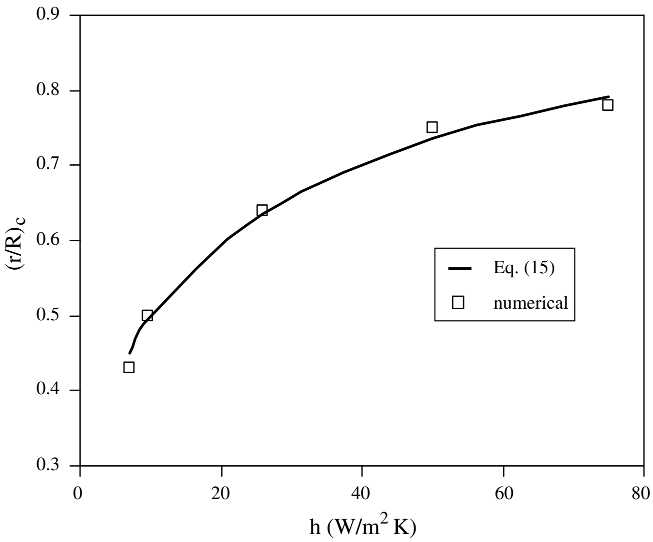

Fig. 8. Critical split radius $(r_1/R)_c$ versus heat transfer coefficient h_{side}, W/m^2 K.

r_c as a function of the side heat transfer coefficient (h_{side}), when compared with the values obtained using numerical simulations. The lowest value for 'h' used in the simulation of the graph (9.58 Wm^{-2} K^{-1}) is calculated by considering only natural convection to take place around the heater, using appropriate correlations from [23]. The next immediate h value (26 Wm^{-2} K^{-1}) is for a typical litho-cell cleanroom case (taken from [9]), while the other increasing 'h' values are done for completion of the comparison. The critical split location for the two-zone compensatory heater, increases with increasing h values and would reach an asymptotic value of $r_c \to 1$ for $h > 100$ Wm^{-2} K^{-1}. At this stage, the method of two-zone compensation is rendered practically invalid and one would require multiple radial-zone compensation.

Fig. 9 displays the effect of varying the h_{side} value on the r_c and the $\Delta\theta_{MIN}$ values along with the corresponding ratio of energies (Q_1/Q_2, marked in right-side y-axis) supplied in the two-zones. As the losses increase the minimum attainable surface temperature also increases. Further, Q_1/Q_2 decreases as losses increase. This implies that Q_2/Q_T increases with increase in losses (because $(Q_1 + Q_2)/Q_2$ also decreases) resulting in an additional energy access to the outer-zone for attaining ΔT_{MIN}. As expected from the earlier discussion, the r_c value reduces for reduction in h_{side}, which can be seen from the curve of Q_1/Q_2 taking positive values from $r_1/R \sim 0.43$ and 0.64 for $h_{side} = 9.6$ and 26 Wm^{-2} K^{-1}, respectively. Further, these non-dimensional $\Delta\theta_{MIN}$ values and the corresponding Q_1/Q_2 values are independent of the T_{SET} chosen. However, the dimensional ΔT_{MIN}, as can be seen from Fig. 6, would be different for different T_{SET} values.

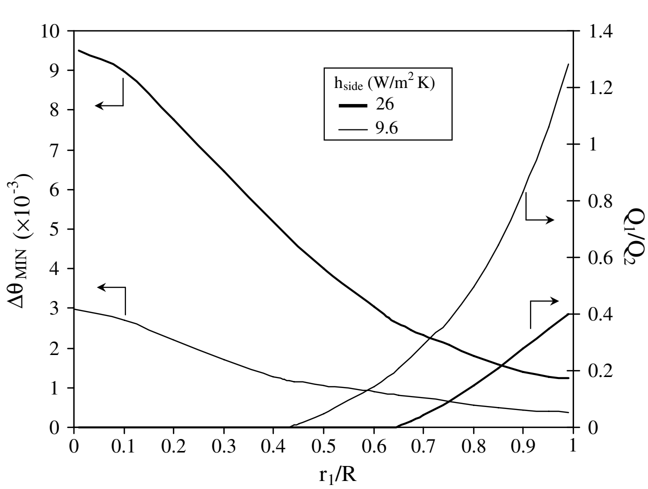

Fig. 9. Variation of heater surface $\Delta\theta_{MIN}$ with r/R and corresponding Q_1/Q_2 for two h_{side}, W/m^2 K.

9. Conclusions

A proposed steady state, inverse method of two-zone heat flux redistribution on the bottom surface to minimize the top surface temperature difference of a disc heater employed in the post-exposure bake process of a 300 mm silicon wafer used in microlithography, the semiconductor manufacturing process, has been studied in detail. The transport equations with realistic boundary convection losses were solved using numerical methods with a finite volume axi-symmetric formulation of the heater domain.

For a chosen T_{SET} and given convection heat losses from the heater edges, the achievable heater surface ΔT_{MIN} decreases as the split location separating the inner- and outer-zone of the theater bottom surface (r_1/R) increases. Further, for a split location (r_1/R) and known constant convection losses (h_{side} and h_{top}), the achievable heater surface ΔT_{MIN} increases with T_{SET}.

There exists a critical split radius ($r_c = (r_1/R)_c$) below which no energy need be given to the inner-zone ($q''_1 = 0$) to achieve the ΔT_{MIN} on the top surface. This critical split radius value is predicted using a theoretical scaling analysis from first principles and was found to match excellently with the value obtained from numerical methods. With corroborative results from the numerical simulations, the scale analysis further revealed for a given disc heater geometry and ambient temperature, the r_c to be independent of the T_{SET} and h_{top} and depends only on h_{side}, the heater edge convection heat transfer coefficient. A knowledge of the r_c is useful while designing such a two-zone heater to determine the spatial allowances required in the inner- and outer-zone electric resistance heater strip densities, as the split located at a position lesser than the r_c, would render the entire inner-zone practically useless for achieving an overall surface ΔT_{MIN}.

The heat flux ratios q''_1/q''_2, and r_c were found to be independent of the T_{SET} and dependent only on the heat losses. This useful conclusion implies the same heater can be used for heating the silicon wafer to any T_{SET}, which varies for the several combinations of the photo-resist and radiation used while imaging the circuit pattern (90 °C < T_{SET} <

250 °C, in general). However, the ΔT_{MIN} obtained would be different for different T_{SET} values. Limiting values of achievable heater surface ΔT_{MIN} in this method of two-zone redistribution of heat flux is also presented.

References

[1] L.F. Thompson, C.G. Willson, M.J. Bowden, Introduction to microlithography, 1st edition., American Chemical Society, Washington, DC, 1983.

[2] L.F. Thompson, C.G. Willson, M.J. Bowden, Introduction to Microlithography, 2nd edition., American Chemical Society Prof. Ref. Book, Washington, DC, 1994.

[3] P. Rai-Choudhury, Handbook of microlithography, micromachining and, microfabrication, SPIE Optical Engineering Press, Bellingham, USA, 1997.

[4] H. Ito, Chemical amplification resists: History and development within IBM, IBM J. Res. Dev. 44 (2000) 119–130.

[5] R. Mohondro, Photostabilization: Comparing DUV and *i*-line, Solid State Technol. (2003) 69–74, February.

[6] M.D. Smith, C.A. Mack, J.S. Peterson, Modeling the impact of thermal history during post exposure bake on the lithographic performance of chemically amplified resists, Proc. SPIE 4345 (2001) 1013–1021.

[7] W.D. Hinsberg, F.A. Houle, M.I. Sanchez, G.M. Wallraff, Chemical and physical aspects of the post-exposure baking process used for positive-tone chemically amplified resists, IBM J. Res. Dev. 45 (5) (2001) 667–682.

[8] J. Beck, B. Blackwell, C. St-Clair Jr., Inverse heat conduction: Ill-posed problems, Wiley InterScience, New York, 1985.

[9] A. Narasimhan, N. Ramanan, Simulation studies and experimental verification of the performance of a litho-cell combination bake-chill station, J. Microlith. Microfab. Microsys. 3 (2) (2004) 332–338.

[10] J. Lewellen, E. Gurer, E. Lee, L. Chase, L. Dulmage, Effect of PEB temperature profile on CD for DUV resists, Proc. SPIE 3882 (1999) 45–54.

[11] K. El-Awady, C.D. Schaper, T. Kailath, Programmable thermal processing module for semiconductor substrates, IEEE Trans. Control Syst. Technol. 12 (4) (2004) 493–509.

[12] C.D. Schaper, K. El-Awady, T. Kailath, A. Tay, L.L. Lee, W.K. Ho, S.E. Fuller, Processing chemically amplified resists on advanced photomasks using a thermal array, Microelectron. Eng. 71 (1) (2004) 63–68.

[13] A. Tay, W.K. Ho, N. Hu, X.Q. Chen, Estimation of wafer warpage profile during thermal processing in microlithography, Rev. Sci. Instrum. 76 (7) (2005) 1–7.

[14] N. Ramanan, F. Liang, J. Sims, Conjugate heat-transfer analysis of 300-mm bake station, Proc. SPIE 3678 (1999) 1296–1306.

[15] N. Ramanan, A. Kozman, J. Sims, On the differences between wafer and bake plate uniformity in proximity bake, Adv. Resist Process. Proc. SPIE 3999 (2000).

[16] W.H. Ho, A. Tay, C.D. Schaper, Optimal predictive control with constraints for the processing of semiconductor wafers on bake plates, IEEE Trans. Semicond. Manuf. 13 (1) (2000) 88–96.

[17] W.W. Tan, R.F.Y. Li, An in-situ temperature measurement system for DUV lithography, IEEE Trans. Instrum. Meas. 52 (4) (2003) 1136–1142.

[18] A. Tay, W.K. Ho, A.P. Loh, K.W. Lim, W.W. Tan, C.D. Schaper, Integrated bake/chill module with in situ temperature measurement for photoresist processing, IEEE Trans. Semicond. Manuf. 17 (2) (2004) 231–242.

[19] A. Narasimhan, N. Ramanan, D. Williams, Performance Evaluation and Analysis of a Novel 300-mm Combination Bake-Chill Station, Adv. Resist Technol. Process. XX, Proc. SPIE 5039 (2003).

[20] C.H. Huang, T.M. Ju, A.A. Tseng, The estimation of surface thermal behavior of the working roll in hot rolling process, Int. J. Heat Mass Transfer 38 (6) (1995) 1019–1031.

[21] H.M. Park, W.S. Jung, Recursive solution of an inverse heat transfer problem in rapid thermal processing systems, Int. J. Heat Mass Transfer 44 (2001) 2053–2065.

[22] K.D. Cole, D.H.Y. Yen, Green's function, temperature and heat flux in the rectangle, Int. J. Heat Mass Transfer 44 (2001) 3883–3894.

[23] A. Bejan, Convection heat transfer, 2nd edition., Wiley and Sons, 1995.